Olivine dissolution in seawater: implications for CO_2 sequestration through Enhanced Weathering in coastal environments

Journal:	*Environmental Science & Technology*
Manuscript ID	es-2016-059426.R3
Manuscript Type:	Article
Date Submitted by the Author:	09-Mar-2017
Complete List of Authors:	Montserrat, Francesc; Vrije Universiteit Brussel, Department of Analytical, Environmental and Geo-chemistry Renforth, Phil; University of Oxford, Earth Sciences Hartmann, Jens; Universitat Hamburg, Department of Earth Sciences Leermakers, Martine; Vrije Universiteit Brussel, Department of Analytical, Environmental and Geo-chemistry Knops, Pol; Green Minerals B.V. Meysman, Filip; Vrije Universiteit Brussel, Department of Analytical, Environmental and Geo-chemistry; Aarhus Institute for Advanced Studies

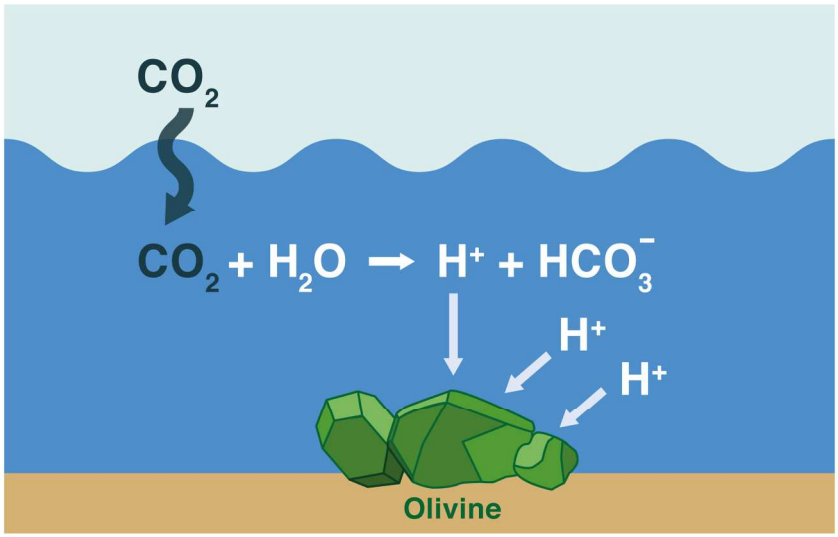

TOC art
TOC art
165x114mm (300 x 300 DPI)

Olivine dissolution in seawater: implications for CO_2 sequestration through Enhanced Weathering in coastal environments

Author names

Francesc Montserrat[*,1,6], Phil Renforth[2], Jens Hartmann[3], Martine Leermakers[1], Pol Knops[4] and Filip J.R. Meysman[1,5]

Author addresses

(*) Corresponding Author, montserrat@usp.br, f.montserrat@gmail.com ;

(1) Department of Analytical, Environmental and Geo-Chemistry, Free University of Brussels, Pleinlaan 2, 1050, Brussels, Belgium;

(2) School of Earth and Ocean Sciences, Cardiff University, Main Building, Park Place, Cardiff, CF10 3AT, United Kingdom;

(3) Institute for Geology, Center for Earth System research and sustainability (CEN), Universität Hamburg, Bundesstraße 55, 20146, Hamburg, Germany;

(4) Green Minerals B.V., Boulevard 17, 6127 AX, Grevenbicht, The Netherlands;

(5) Aarhus Institute of Advanced Studies (AIAS), Aarhus University, Hoegh-Guldbergs Gade 6B, DK-8000 Aarhus C, Denmark

(6) Current Address: Department of Marine Ecology, Management and Conservation, Institute for Oceanography – University of São Paulo, Praça do Oceanografico 191, 05508-120, São Paulo (SP), Brazil

Keywords

Climate Change, Ocean Acidification, Geo-engineering, Carbon Dioxide Removal, Enhanced Mineral Weathering, Alkalinity, DIC

Abstract

Enhanced Weathering of (ultra)basic silicate rocks such olivine-rich dunite has been proposed as a large-scale climate engineering approach. When implemented in coastal environments, olivine weathering is expected to increase seawater alkalinity, thus resulting in additional CO_2 uptake from the atmosphere. However, the mechanisms of marine olivine weathering and its effect on seawater carbonate chemistry remain poorly understood. Here, we present results from batch reaction experiments, in which forsteritic olivine was subjected to rotational agitation in different seawater media for periods of days to months. Olivine dissolution caused a significant increase in alkalinity of the seawater, with a consequent DIC increase due to CO_2 invasion, thus confirming viability of the basic concept of enhanced silicate weathering. Yet, our experiments also identified several important challenges with respect to the detailed quantification of the CO_2 sequestration efficiency under field conditions, which include non-stoichiometric dissolution, potential pore water saturation in the seabed, and the potential occurrence of secondary reactions. Before enhanced weathering of olivine in coastal environments can be considered an option to realize negative CO_2 emissions for climate mitigation purposes, these aspects need further experimental assessment.

Introduction

Climate engineering approaches that aim to deliberately and actively remove greenhouse gasses from the atmosphere are categorized as Carbon Dioxide Removal (CDR) or Negative Emission Technologies (NETs)[1]. CDR or NETs are seen as a possible future complement to current climate policies, which are presently only focused on the reduction of CO_2 emissions. Model studies emphasize that the large-scale implementation of NETs will be needed to limit global warming to within a 2°C increase with respect to preindustrial conditions[2,3]. The worldwide commitment to attain this target, thus avoiding a ‘dangerous’ level of climate change, has been strengthened by the recent COP21 Paris Agreement[4].

Enhanced Silicate Weathering (ESW) is a NET approach in which the natural process of (silicate) rock weathering is artificially stimulated[5,6]. The technique has been recognized as a potentially promising strategy for CO_2 removal from the atmosphere, while at the same time counteracting ocean acidification[1,6–9]. The implementation of ESW requires suitable source rock to be mined, ground to small grain sizes and subsequently spread over suitable areas[5]. The mineral grains dissolve (i.e. chemical weathering), through which CO_2 is eventually captured from the atmosphere[6,10]. Olivine ($Mg_{2-x}Fe_xSiO_4$) is an abundant and fast-weathering ultramafic silicate mineral, and has been advanced as a prime candidate mineral for ESW application[5,11]. The dissolution of olivine in an aqueous environment consumes protons or equally increases alkalinity[6,12,13], and so increases CO_2 uptake by the aqueous medium (Supplementary Information SI 1).

In theory, ESW can be applied in terrestrial soils[5,6], in the surface mixed layer of the open ocean[13], or by spreading minerals onto sediments of the coastal zone and continental shelf[14]. The largest application domain for ESW would be the open ocean, but model analysis suggests that the olivine particles need to be ground to very small sizes to facilitate dissolution in the surface ocean[13]. As such, the high grinding costs and CO_2 emissions during production potentially limit this approach. An alternative scheme is the application of ESW to coastal and shelf environments, where it could be integrated into existing coastal zone management practices, such as dredging operations, land reclamation, and beach nourishment. A theoretical examination of the concept of coastal ESW [14] has indicated advantages as well as challenges. One important knowledge gap is that detailed experimental investigations of olivine dissolution under natural conditions (i.e. realistic for coastal ESW) are lacking. A better understanding of the rate and mechanism of olivine dissolution in natural marine environments is needed, in order to better evaluate the feasibility and potential of coastal ESW as a NET. Previous work has largely focused on olivine dissolution under laboratory conditions using artificial seawater solutions[15–18]. Such idealized approaches potentially exclude important geochemical and environmental influences that could be relevant under field conditions.

Here we specifically address a number of questions related to the application of enhanced silicate weathering in natural coastal environments: (1) What is the rate of olivine dissolution in natural seawater and how does this differ from artificial seawater? (2) Does olivine dissolve stoichiometrically in natural seawater? (3) What dissolution products can be used to efficiently monitor the dissolution rate of olivine in coastal sediments, i.e., quantify the efficiency of enhanced silicate weathering? (4) To what extent does secondary mineral formation diminish the CO_2 sequestration efficiency of olivine dissolution in seawater?

We present results from dissolution experiments with simulated grain-grain collisions, in which olivine was dissolved in natural filtered seawater as well as in artificial seawater media with modified cation composition. Potential proxies for quantifying the dissolution rate of olivine are analyzed and compared. Based on these results, we discuss a number of challenges for ESW in coastal environments.

Materials and Methods

Materials

Commercially available olivine sand ($Mg_{2-x}Fe_xSiO_4$) and lab-grade quartz (SiO_2) were used in slurry dissolution experiments. The olivine sand (particle size quantiles: D10 = 91 μm, D50 = 143 μm, D90 = 224 μm) had a molar Mg:Fe ratio of 0.94:0.06, characterizing the olivine as Forsterite-94 (Fo_{94}). The Ni content was estimated at 0.0075 mol Ni mol^{-1} olivine. Further details on the chemical composition, grain size distribution and pre-experimental treatment are summarized in Tables S1 and S2 (SI 2).

Different reactive seawater media were used as supernatant. Filtered seawater (FSW) was collected as natural seawater from the Oosterschelde tidal basin (The Netherlands) and filtered over a Mahle amaGuard FP 0.2 [μm] woven cotton filter (Mahle Benelux, The Netherlands). In addition, three types of artificial seawater were prepared according to the ASTM Standard Practice D 1141-

98[19] (Table S3): 1) plain artificial seawater (ASW), 2) artificial seawater with Ca^{2+} replaced by Na^{+} (hereafter named ASW-Ca) and 3) artificial seawater with both Ca^{2+} and Mg^{2+} replaced by Na^{+} (hereafter named ASW-CaMg).

Experiments

Specific amounts of olivine and quartz grains were added to a specific volume of seawater in 500 ml boro-silicate glass bottles, which were then subjected to continuous rotating movements on a CH-4103 rotating shaking platform (INFORS AG, Switzerland) set at 155 rpm. The bottles were closed with membrane screw caps, equipped with a 0.5 mm thick silicone septum that prevented evaporation, but allowed gas exchange. To prevent photosynthesis, the experiment took place in the dark, while the bottles were wrapped in aluminium foil (leaving the top of the membrane cap uncovered).

Three types of agitation experiments were conducted: A1, A2 and A3 (SI 3, Table S4). In both the A1 and A2 experiments, 0.1 mol of either olivine (OLI) or quartz (QUA) were added to 300 ml FSW, with one control treatment (i.e. only seawater; SW). Three replicates were conducted per treatment (n = 3). Experiment A1 was conducted under ambient conditions, i.e. without regulation of temperature (range: 13.5 – 20°C) and pCO_2 (range: 445 – 525 ppmv), and lasted for 88 days. The second agitation experiment, A2, had essentially the same setup as A1, except for a few modifications. Firstly, natural seawater was bubbled with air prior to the experiment, to ensure CO_2 equilibration with the surrounding atmosphere. Secondly, the experiment had a much shorter duration (20 days) and it was conducted under stable temperature and pCO_2 conditions. The third experiment, A3, was designed to specifically investigate the effect of the composition of seawater on the dissolution rate of olivine (quartz was not investigated). Agitation experiment A3 was designed to examine the effect of the composition of seawater on the dissolution rate. A3 was also conducted under stable temperature and pCO_2 conditions and used atmosphere-equilibrated reactive fluids, bubbled with air. The dissolution of olivine (OLI) was monitored in four reactive fluids

(FSW, ASW, ASW-Ca, ASW-CaMg; SI 2) and compared to control treatments (respective solution media without olivine). Instead of 0.10 mol olivine used in A1 and A2, 0.03 mol was used in A3 (Table S3).

To test the impact of agitation, a layer of olivine sand was placed also in a non-moving cylindrical container with FSW (n=1). In this non-agitated treatment the olivine itself was not agitated. Rather, the overlying water was stirred and only samples for solid phase analysis were collected.

Water and solid phase analysis

The overlying water of the slurry batch reaction experiments was sampled at regular time intervals and analyzed for temperature, salinity, pH, total alkalinity (TA), dissolved inorganic carbon (DIC), dissolved silicate (Si), dissolved Nickel (Ni) and dissolved Magnesium (Mg), using standard analytical procedures[20,21] (SI 3). All solute concentrations are reported as micromole per kilogram seawater [μmol kg^{-1}].

Upon completion of the A3 experiment, olivine grains were recovered from the agitated and non-agitated treatments, inspected for dissolution features and analyzed for carbonate precipitates, according to Nieuwenhuize et al. [20], to yield the mass percentage of inorganic carbon (mass% C_{inorg}). The elemental composition of the olivine particle surfaces were investigated using scanning electron microscope energy-dispersive X-ray spectroscopy (SEM-EDX).

Additional details on both water and solid phase analyses can be found in SI 3.

Olivine dissolution rate calculations and simulations

The accumulation over time of the reaction products in the reactor vessels is reported as excess concentration values, $\Delta C_i(t) = C_{treatment}(t) - C_{control}(t)$. In this, the control refers to the treatment without the addition of any solid minerals. Three empirical mathematical models were implemented

to describe $\Delta C_i(t)$ as a function of the incubation time, and from these model fits the accumulation rate R_i [μmol kg^{-1} d^{-1}] of compound i and the associated area-specific dissolution rate constant k_i, [μmol m^{-2} d^{-1}] were derived (SI 4). Note that in the case of stoichiometric dissolution, the rate constants k_i should be -at least in theory- identical for all olivine dissolution products.

The accumulation of weathering products and the change of solution chemistry during the batch dissolution experiments was also mechanistically simulated using the geochemical software package PHREEQC v2 [22]. In these simulations, the solution chemistry (and hence the saturation states) were free to evolve with time as a consequence of mineral dissolution (kinetic rate equations specified in SI 4). Solubility constants were taken from the MINTEQ.dat and LLNL.dat databases to calculate the saturation states of solid phases in the solution. The measured initial composition of the solution, which was specific for each treatment, was used as the starting conditions for the PHREEQC simulations.

All mathematical analyses, apart from the PHREEQC analyses, and plotting were done using the open source R framework for statistical computing[23].

Results

Olivine and quartz dissolution in natural filtered seawater

In the A1 and A2 experiments, we investigated the dissolution of olivine and quartz in natural filtered seawater.

In both A1 and A2, there was a clear ΔSi signal in the quartz treatment (QUA), most likely caused by dissolution of very fine quartz particles (Fig. 1). ΔSi increased until ~18 μmol kg^{-1} within the first week of the experiments, after which it remained constant. There was no discernible Ni release in the A1 and A2 quartz treatment (Fig. 1), and hardly any response from the carbonate

system. The ΔpH increased by 0.05 within the first two weeks, but then decreased again to its initial value by the end of the experiment. While ΔTA remained constant with time, ΔDIC decreased with 22 μmol kg^{-1} during the first 15 days, likely caused by CO_2 outgassing, as the initial solution in A1 may not have been in equilibrium with the atmosphere (SI 2 and SI 3). In the A2 experiment, the experimental procedure was improved, and the FSW medium was bubbled with ambient air at the start of the experiment. As a result, the carbonate system variables ΔDIC, ΔTA or ΔpH did not change significantly over time (linear regression, $p = 0.35$, $p = 0.28$ and $p = 0.696$, respectively).

In the olivine treatment (OLI) of experiment A1, increases with time of both ΔSi and ΔNi were observed, suggesting olivine dissolution (Fig. 1). While ΔNi levelled off at 3.2 μmol kg^{-1}, suggesting that an equilibrium was reached, ΔSi increased almost linearly over the 88-day incubation period, displaying a much stronger dissolution than in the QUA treatment. Experiment A2 showed a similar temporal evolution of ΔSi and ΔNi (Fig. 1). ΔTA showed a pronounced increase over the first 5 days (Fig. 1), levelling off thereafter at ΔTA = 103 μmol kg^{-1}. ΔDIC increased in a similar way, albeit over a slightly longer period of ~15 days, levelling off at ΔDIC = 93 μmol kg^{-1}. The pH in the olivine treatment increased rapidly over the first 5 days by ~ 0.1, after which it decreased again and levelled off at ΔpH = 0.02 (Fig. 1). The carbonate system in A2 showed a similar pattern, ΔTA and ΔDIC levelling off at 104 and 74 μmol kg^{-1}, respectively (Fig. 1). Similar to experiment A1, the ΔpH in A2 increased strongly within the first 6 days by ~ 0.15, after which it decreased again to ΔpH = 0.06 (Fig. 1).

Olivine dissolution in artificial seawater media with different cation composition

In experiment A3, large differences in the release of dissolution products were observed between the different seawater media. All four media displayed a quasi-linear ΔSi response with time (Fig. 2). The ΔSi attained at the end of the experiment was lowest in the natural seawater (FSW: 68 μmol Si kg^{-1}) and artificial seawater (ASW: 82 μmol Si kg^{-1}), and increased markedly when Ca^{2+} and Mg^{2+} were replaced by Na^{+} in the medium (ASW-Ca: 122 μmol Si kg^{-1}; ASW-CaMg:

162 μmol Si kg^{-1}).

The Ni release showed a saturation-type response, which varied between media. In the FSW, ASW and ASW-Ca treatments (Fig. 2), the ΔNi concentration showed a comparable accumulation (plateau concentrations between 1.19 and 1.68 μmol Ni kg^{-1}). In contrast, the ASW-CaMg treatment showed hardly any Ni accumulation, apart from a small initial release, which was taken up again by the end of the experiment.

The carbonate system (TA, pH and DIC) responded very differently in the Ca/Mg-free seawater compared to the three other treatments. Although the shape of the response curves were similar, the overall accumulation of alkalinity (ΔTA = 340 ± 14 μmol kg^{-1}) and dissolved inorganic carbon (ΔDIC = 317 ± 11 μmol kg^{-1}) was substantially higher in the ASW-CaMg compared to the other treatments (range ΔTA = 41 – 69 μmol kg^{-1} and ΔDIC = 31 – 66 μmol kg^{-1} in FSW, ASW and ASW-Ca). The ΔTA and ΔDIC in ASW-CaMg quickly increased over the first 10 days, after which the increase rate slowed down and the accumulation became linear. The long-term accumulation, i.e. between 30 and 137 days, was higher for DIC (168 ± 50 μmol kg^{-1}) than for TA (127 ± 12 μmol kg^{-1}).

The ΔpH showed an "overshoot" response, with a sharp initial increase in the first 5 days, reaching maximum between 4 and 7 days, after which the ΔpH gradually decreased and tended towards an asymptotic equilibrium value at the end of the experiment (Fig. 2). Consistent with the stronger alkalinity accumulation in the Ca/Mg-free seawater, the long-term pH (pH_{t137} minus pH_{t0}) increase was much higher in the Ca/Mg-free seawater (ΔpH = 0.06), compared to the other three treatments (range in ΔpH = -0.01 to 0.035 at 137 days).

Olivine dissolution stoichiometry and rates

PHREEQC kinetic modelling of the ASW, ASW-Ca and ASW-CaMg treatments, suggested that all reactive fluid media in experiment A3 were undersaturated for forsterite ($\Omega_{forsterite} = 10^{-5}$ for FSW, ASW, and ASW-Ca and $\Omega_{forsterite} = 10^{-10}$ for ASW-CaMg).

The accumulation rates R were determined by the best model fit [23] (see Fig. S6 for representative examples) to the response curves of the olivine dissolution products ΔSi, ΔNi, ΔMg and ΔTA and the ensuing CO_2 sequestration ΔDIC (Table 1). As emphasized above, different dissolution products tended to have different response curves within the same treatment, thus indicating non-stoichiometric dissolution (Table 1). In the case of ΔSi, the accumulation response was generally best described by a linear model (model 1, Table S5), while for ΔTA, ΔDIC, ΔMg and ΔNi the profiles were typically best fitted with a saturation model (model 2, Table S5), or a combination of short-term saturation with a long-term linear increase (model 3, Table S5). Only in the ASW-CaMg treatment (experiment A3), all variables could be described best by model 3 (Table S5)

To further illustrate the absence of stoichiometric dissolution in either natural or artificial seawater in the presence of magnesium, Figure S8 plots the accumulation of response variables in experiment A3 normalized for stoichiometry (Table S1: ΔSi/1, ΔTA/4, ΔNi/0.0075, ΔMg/1.87). Only in the ASW-CaMg treatment, olivine dissolution tends to become stoichiometric, as shown by the similar responses for ΔMg and ΔTA (Fig. S8).

Because of non-stoichiometric dissolution, the olivine dissolution rate constant k_i showed a dependence on the response variable (ΔSi, ΔNi, ΔMg, ΔTA and ΔDIC; Table 2). The rate constant based on ΔNi ($k_{\Delta Ni}$) is the highest of all response variables and is similar across all treatments (31-74 μmol olivine m^{-2} d^{-1}). In the ASW-CaMg treatment, $k_{\Delta Mg}$ (63 μmol olivine m^{-2} d^{-1};) were consistent with $k_{\Delta Ni}$ values, while $k_{\Delta Si}$ were an order of magnitude lower than $k_{\Delta Ni}$ values in the reactive fluid media containing Mg^{2+} (Table 1 and 2). The exclusion of Mg^{2+} in the Mg-free reactive fluid (ASW-CaMg), increased $k_{\Delta Si}$ by one order of magnitude. The values of both $k_{\Delta TA}$ and $k_{\Delta DIC}$ show substantial variation between treatments, and are highest in the ASW-CaMg treatment. The temperature-normalized [24] (to 25° C) mean values for k_i (where i = ΔSi, ΔNi, ΔTA, ΔDIC), for the FSW and ASW cases are shown in Fig. 3 (the ASW-Ca and ASW-CaMg treatments are considered unrealistic for ESW and thus excluded).

253

254 **SEM-EDX**

255 SEM-EDX analyses of mineral grains from fresh, unreacted olivine were generally angular,
256 with sharp edges (Fig. 4A). In contrast, olivine grains that had been rotating during the entire
257 experiment (137 d) were generally sub-rounded (Fig. 4B), suggesting abrasion due to grain-grain
258 collisions. The Mg:Si atomic ratios (Mg:Si) at the surface of the unreacted particles were
259 significantly higher (mean±SEM Mg:Si = 2.11±0.02, n_{grains} = 6; Fig. S9) than for grains that were
260 agitated in solution (mean±SEM Mg:Si 1.7±0.04 – 2±0.03, n_{grains} = 3-10; Fig. S9). This suggests
261 preferential mobilization of Mg during dissolution, consistent with the higher dissolution rates
262 obtained for Mg and Ni, compared to Si. The preferential leaching of Mg^{2+} (lowest Mg:Si ratio) was
263 most prominent in the ASW-CaMg treatment (Figure S10), where areas with Mg:Si ≤ 1 and lower
264 were observed. No carbonate minerals were observed on any of the analyzed olivine grains.

265

266 **Potential for carbonate precipitation**

267 The inorganic carbon content (C_{inorg}) in the solid mineral phase recovered from
268 experiment A3 was very low (mean C_{inorg} < 0.005 %) and was not significantly different between the
269 four treatments (one-way ANOVA, p = 0.112; Figure S9). Small changes in the solid phase
270 carbonate content (which are difficult to measure) could nevertheless be associated with substantial
271 changes in the alkalinity of the supernatant. Although not significantly different, the difference in
272 C_{inorg} content between FSW and ASW-CaMg was 0.003 mass%. If this difference would be real and
273 caused by carbonate precipitation, this would imply that the FSW contained 37 μmol kg^{-1} of $CaCO_3$
274 in excess to the ASW-CaMg, when expressed per unit volume of fluid. The absence of this
275 precipitation would hence cause the alkalinity to be 74 μmol kg^{-1} higher in ASW-CaMg. However,
276 the measured ΔTA difference between the ASW-CaMg treatment and the FSW/ASW was much
277 higher, amounting to ca. 300 μmol TA kg^{-1} at the end of experiment A3 (Fig. 2). Accordingly,

carbonate precipitation cannot explain the difference in alkalinity between the FSW and ASW-CaMg treatments, and so likely, more olivine dissolution took place in the ASW-CaMg treatment.

Discussion

The dissolution experiments here demonstrate several features regarding olivine weathering in seawater and its potential applications for ESW in coastal settings. Firstly, the basic principle underlying ESW in seawater appears to work. Olivine dissolution in natural seawater under non-sterile laboratory conditions consistently causes alkalinization, followed by CO_2 invasion from the atmosphere into the seawater, at rates in agreement with those estimated by previous studies[14,24,25]. Secondly, apparent non-stoichiometric dissolution complicates the experimental determination of the rate and extent of olivine dissolution within the seabed, making it more challenging to assess of the efficiency of ESW. Therefore, the quantification of the actual olivine dissolution rate under realistic *in situ* conditions will require a multi-parameter approach, combining flux measurements of dissolved silicate, dissolved metals (nickel, iron) and alkalinity, with appropriate experimental controls. Thirdly, the rate of olivine dissolution within the seabed can be limited by saturation effects, which could decrease the efficiency of ESW applications. Fourthly, the extent to which secondary reactions impact the CO_2 sequestration efficiency of olivine dissolution under *in situ* conditions remains unresolved and is an important issue to address in further studies on coastal ESW. We will now discuss each of these aspects in more detail.

Quantification of the olivine dissolution rate

In order to be implemented as a Negative Emission Technology (NET) for climate change mitigation[7], the carbon sequestering potential of marine olivine dissolution needs to be quantified.

In other words: How much olivine dissolution occurs within the seabed? What is the time frame n which olivine particles react? How much CO2 is eventua lly taken up by the seawater as a conseq ence of ESW?

The overall CO_2 sequestration rate (R_{CO_2} ; mol CO_2 per m^2 of seabed per unit of time) can be expressed as:

(1) $R_{CO_2} = \gamma_{CO_2} R_{OLI} = \gamma_{CO_2} (k_{OLI} A_{surface} C_{OLI})$

To determine the effectiveness of coastal ESW, both the factors γ_{CO_2} and R_{OLI} need to be accurately constrained. The CO_2 sequestration efficiency γ_{CO_2} specifies the net amount of CO_2 that is taken up from the atmosphere during the dissolution of 1 kg of olivine within the seafloor (this parameter will be further discussed below). For a given amount of finely ground olivine distributed onto the seafloor (C_{OLI} ; mol olivine m^{-2} of seabed), the olivine dissolution rate (R_{OLI} ; mol olivine per m^2 of seabed per unit of time) determines over what time frame the ESW application will be effective (dissolution period $\tau = C_{OLI}/R_{OLI}$). The olivine dissolution rate R_{OLI} further depends on the specific surface area of the mineral grains ($A_{surface}$; m^2 g^{-1}) and the intrinsic dissolution rate constant (k_{OLI} ; mol olivine per m^2 grain surface area per unit of time).

In practical ESW applications, the olivine dissolution rate (R_{OLI}) within the seabed can be determined experimentally by monitoring the release of olivine dissolution products from the seabed. This poses the question as to which dissolution product (e.g. Mg^{2+}, Si, TA) should be monitored as a reliable proxy for the olivine dissolution rate in field-type experiments. The use of both dissolved silicate and alkalinity is non-trivial as these are generated in sediments by other processes than olivine dissolution[26]. Any observed sediment efflux of dissolved silicate and alkalinity can thus not be exclusively attributed to olivine dissolution. Furthermore, Mg^{2+} cannot be used as a dissolution proxy, due to the high background concentration in seawater (~ 50 mmol Mg^{2+} kg^{-1} seawater), and so, its accumulation in the overlying water cannot be reliably measured.

Our experiments suggest that Ni^{2+} could be a suitable dissolution proxy, generating a

dissolutive accumulation, which substantially supersedes the ambient seawater concentration[27,28] (0.002 - 0.16 µmol Ni kg^{-1}). This way, pore water accumulation and sediment fluxes of Ni can be accurately measured using standard analytical techniques for trace metals (e.g. ICP-MS). Yet, to qualify as a good proxy for sedimentary dissolution of olivine, two important conditions need to be fulfilled. Firstly, the efflux of the olivine proxy (Ni) from the sediment should also match the release rate of the weathering products in the pore solution. In this regard, Ni^{2+} seems an advantageous proxy. The natural cycling of Ni^{2+} in coastal sediments is restricted, and so the observed Ni^{2+} efflux from the sediment in olivine addition experiments can be fully attributed to olivine dissolution. Still, in future studies, it should be verified whether the Ni^{2+} release is modulated by diagenetic effects within the sediment (e.g. sorption onto minerals).

A second important condition is that stoichiometric dissolution of olivine occurs, so that the Ni^{2+} release can be properly rescaled to the overall olivine dissolution rate R_{OLI} by means of the Ni content of the olivine source rock that is used[25]. However, our experiments suggest that this not the case (Table 1, 2). The experiments A1-A3 show that, when assessed over short-time scales, the dissolution of olivine in seawater is non-stoichiometric, implying incongruent dissolution under Earth surface conditions[29]. In the absence of secondary precipitation reactions, non-stoichiometric dissolution cannot continue indefinitely. Experiments of longer time scales should therefore clarify to what extent the Ni^{2+} release from sediments can be a valid proxy for in situ olivine dissolution.

In our dissolution experimental the k_i value for Si (determined at the initial time t_0) was ca. 30 times lower compared to that of Ni (or Mg). This suggests a preferential release of divalent cations, respective to silicate. The preferential release of metal cations (Ni^{2+} and Mg^{2+}) compared to Si, and the observed quasi-linear increase in ΔSi are typical for solid state diffusion in silicate minerals[29], which facilitates the formation of a "surface (altered) layer" [30]. The crystal ionic radius of nickel (83 pm) is only slightly smaller than that of magnesium[31] (86 pm) implying that both metal ions will have a similar rate of solid-state diffusion. Both Pokrovsky & Schott [25] and Palandri & Kharaka[22] already suggested that for slightly alkaline solutions (e.g. seawater), forsterite dissolution

353 at steady-state is controlled by the decomposition of a protonated surface complex, which is silica-
354 rich and magnesium-deficient. Maher et al. [32] postulate that olivine dissolution occurs as a series of
355 boundary layer processes, in which primary dissolution of cations is followed by dissolution of
356 silicic acid ions, which may subsequently re-polymerise at the surface. This implies that the
357 measured dissolved silica release rate is a net value, which may not serve as the sole proxy for
358 olivine dissolution. Although in some SEM-EDX images -particularly those from the ASW-CaMg
359 treatment (Fig. S10)- the particle surface did look as if flakes of surface material had been
360 detaching, the examined olivine grains did not show any evidence of secondary silicate
361 precipitates[17,33–35].

362 A significant finding here is that SEM-EDX analyses show decreasing Mg:Si atomic ratios
363 of the forsterite surface between initial substrate and reacted material (Fig. S9). Rather than a build-
364 up of thick silica formations, these decreasing Mg:Si ratios corroborate the mechanism of a cation-
365 leached, surface altered layer formation by preferential dissolution and subsequent re-
366 polymerization processes *sensu* Hellmann et al. [30] and Maher et al. [32]. The timescale on which the
367 weathering takes place in this study is much longer than in high-temperature/high-pressure studies,
368 or studies in which an elevated pCO_2 is employed[29]. This so-called "unstrained dissolution" [36],
369 combined with physical disturbances -such as grain abrasion- does not allow for the buildup of a
370 conspicuous passivating layer or thick silicate precipitates.

371 The non-stoichiometric dissolution as observed in the experiments here emphasizes that the
372 proper quantification of olivine dissolution in field-type ESW experiments requires a careful
373 experimental design. Overall, the non-stoichiometric dissolution of olivine makes the experimental
374 assessment of ESW more challenging. One cannot simply measure one dissolution proxy (e.g. Ni^{2+})
375 and estimate the release of other reaction products by application of reaction stoichiometry.
376 Moreover, both dissolved silicate and alkalinity are generated in sediments by other processes than
377 olivine dissolution[26]. From a biogeochemical perspective, it is crucial to know how olivine
378 dissolution stimulates the efflux of dissolved silicate and alkalinity from the seabed, because the

efflux of alkalinity is the ultimate driver of CO_2 uptake[37], while silicate could stimulate primary productivity by marine diatoms. Hence, a multi-parameter assessment, combining flux measurements of Ni^{2+}, dissolved silicate and alkalinity, with appropriate experimental controls, seems to provide the best strategy to confidently determine the olivine dissolution rate under *in situ* conditions.

Impact of saturation

The values for the dissolution rate constant k of olivine in seawater obtained in this study, are consistent with literature values. For the temperature ranges used in FSW and ASW, the dissolution rate constant varied between 1.9±0.8 µmol olivine m^{-2} d^{-1} for k_{Si} and 56±18 µmol olivine $m^{-2}d^{-1}$ for k_{Ni} (mean±SD values). Normalized for temperature differences, these k value ranges corresponded well with the mean value of 14 µmol olivine $m^{-2}d^{-1}$, as compiled by Palandri & Kharaka[22] and Hangx & Spiers[14], of which the latter had an order of magnitude of variation around the mean (Fig. 3).

The non-stoichiometric dissolution in the seawater media FSW and ASW, together with the saturation behavior observed in the TA, Mg^{2+} and Ni^{2+} results (Fig. 1), suggest that the olivine dissolution approached thermodynamic equilibrium, thus slowing down the reaction. Only by using a lower solubility product for forsterite ($\log K$ = 26.448) than those found in the PHREEQC databases, model simulations indeed showed a slowing of the dissolution reaction by saturation, mirroring our experimental observations. Furthermore, the DIC accumulation followed that of alkalinity perfectly in all cases, albeit with a time lag. This lag is due to the relatively slow process of CO_2 invasion[38], and is also observed in the pH response, which first increases to reach a maximum and then subsequently decreases again. This pH response reflects the initial removal of protons through olivine dissolution, followed by a replenishment of the proton pool by lagged CO_2 transfer.

The observed time response of the reaction products in our experiments provide a first idea

about the possible influence of saturation effects under *in situ* conditions. Our experiments show that saturation occurs within a time frame of about 20 days (Figs. 1 and 2), for an experimental setup with 15 g of olivine in 300 mL of seawater (i.e. 20 mL solution g^{-1} olivine). Assuming the same dissolution rate occurs under *in situ* pore water conditions, the ratio of pore solution to olivine will be lower. For example, if 10-20% of the solid sediment consists of olivine (mixing a 1-2 cm olivine layer into the top 10 cm of sediment), and assuming a porosity of 0.8 and an olivine particle density of 3.3 g mL^{-1}, we obtain a ratio of 6-12 mL solution g^{-1} olivine. Based on our results, such a pore solution will be saturated within 4.5 to 9 days, after which olivine dissolution will slow down and cease. However, the pore water of coastal sediments is also regularly refreshed through physical, advective pore water flow induced by waves and currents[39] and/or biological irrigation by burrowing macrofauna[40,41]. Coastal sediments subject to moderate/high bio-irrigation show flushing rates in the range of 10-100 L m^{-2} day^{-1} [39], implying that the pore solution of the first 10 cm would be refreshed on a time scale of 0.5-8 days (assuming a porosity range from 0.5 to 0.8). In these sediments, irrigation appears sufficient to counteract the saturation of olivine dissolution in the pore water. However, in more cohesive (muddy) coastal sediments with flushing rates < 10 L m^{-2} day^{-1}, saturation effects can be expected, which could decrease the efficiency of enhanced olivine weathering applications. Therefore, a judicious choice of the application location seems warranted[42].

CO_2 sequestration efficiency

The experiments in this study were performed in a set-up that allowed free gas exchange with the atmosphere, while internal biological processes affecting the DIC pool were excluded (i.e. primary production and microbial degradation of organic matter) [26,37]. Accordingly, the observed DIC increase in the experiments can be entirely attributed to CO_2 invasion induced by olivine dissolution, illustrating the proof-of-principle that ESW enhanced silicate weathering works as a NET .

The CO_2 sequestration efficiency expresses the amount of CO_2 transferred across the air-sea

interface per unit mass of silicate rock that dissolves within the seabed, and can be written as:

(2) $$\gamma_{CO_2} \equiv \frac{R_{CO_2}}{R_{OLI}} = \frac{R_{CO_2}}{R_{TA}} \frac{R_{TA}}{R_{OLI}} = \left(\partial \Sigma CO_2 / \partial TA\right)_{pCO_2} \frac{R_{TA}}{R_{OLI}}$$

This formulation reflects the two consecutive steps in the process of CO_2 sequestration. In a first step, olivine dissolution takes place (rate R_{OLI}), which increases alkalinity in the pore solution (rate R_{TA}). This alkalinity increase will then shift the acid-base equilibrium from dissolved CO_2 to bicarbonate and carbonate, thus stimulating a CO_2 uptake from the atmosphere across the air-sea interface (rate R_{CO_2})[26,37]. The CO_2 sensitivity $\left(\partial \Sigma CO_2 / \partial TA\right)_{pCO_2}$ specifies how much CO_2 is taken up from the atmosphere for each mole of alkalinity that is released from the seabed. This thermodynamic factor is evaluated at a given partial pressure of CO_2 in the atmosphere, and is dependent on the local salinity, temperature and chemical composition of the coastal seawater[43]. Calculating the CO_2 sensitivity over the entire experimental period, and for all the experiments that had full ionic strength of seawater (A1, A2, A3:FSW and A3:ASW), we obtain a CO_2 sensitivity of 0.84±0.1 [mol DIC mol^{-1} TA], which is in close agreement with the theoretical value 0.854 for seawater at the experimental conditions employed (T = 17°C, S= 33, TA = 2400 µmol L^{-1}, pCO_2 = 400 ppmv)[44].

Accordingly, the CO_2 uptake in our experiments appears entirely congruent with the standard acid-base thermodynamics of the carbonate system in seawater. Nevertheless, the alkalinity increase during olivine dissolution R_{TA}/R_{OLI}, was less than expected. Traditionally, olivine dissolution is described by the reaction equation:

(3) $$Mg_{2(1-x)}\,Fe_{2x}SiO_4 + 4\,H^+ \rightarrow 2(1-x)\,Mg^{2+} + 2x\,Fe^{2+} + H_4SiO_4$$

As four moles of protons are consumed per mole of olivine dissolved, and hence 4 moles of alkalinity are produced, a ratio $\Delta TA/\Delta Si = 4$ ($R_{TA}/R_{OLI} = 4$) is expected. Only in the ASW-CaMg treatment, the $\Delta TA/\Delta Si$ approached the expected value of 4, while it was substantially less in the FSW, ASW and ASW-Ca treatments. These observations suggests that the Equation (3) does not provide a complete description of the overall olivine dissolution process, but that secondary

456 reactions could be active. Overall, CO_2 sequestration efficiency can be formulated as:

457 (4) $\gamma_{CO_2} = 4(\Delta\Sigma CO_2/\Delta TA)(1-x)$

458 Here, 4 denotes the theoretical stoichiometry between olivine dissolution and CO_2 [5,14], and x denotes
459 a reduction in the CO_2 sequestration efficiency due to secondary reactions. Since our slurry
460 experiments were conducted with oxygenated seawater, one such possible reaction is the aerobic
461 oxidation of ferrous iron:

462 (5) $Fe^{2+} + ¼\ O_2 + 1½\ H_2O \rightarrow FeOOH + 2H^+$

463 This re-oxidation process produces free protons, thus consuming again the alkalinity generated
464 during dissolution of the Fe-component of olivine. The olivine employed here contains 6% of Fe
465 (Table S1), which would reduce the alkalinity release by an equal percentage. However, this
466 reduction is not enough to explain the observed $\Delta TA/\Delta Si$ values. Another possibility to reduce
467 the $\Delta TA/\Delta Si$ ratio is calcium carbonate precipitation:

468 (6) $Ca^{2+} + 2\ HCO_3^- \rightarrow CaCO_3 + CO_2 + H_2O$

469 Although the supernatant in the FSW and ASW was saturated with respect to calcite and aragonite,
470 magnesium is known to act as an inhibitor for $CaCO_3$ nucleation in seawater, limiting its
471 precipitation[45,46]. Moreover, exclusion of Ca^{2+} and Mg^{2+} from the ASW-CaMg (SI 3) implied a
472 strong undersaturation with respect to calcium and magnesium carbonate, thus preventing carbonate
473 precipitation. Additionally, our SEM-EDX analyses did not reveal carbonate minerals on the surface
474 of olivine grains, while at the end of the dissolution experiment no significant increase in the
475 inorganic carbon (carbonate) content of the solid phase was observed. Accordingly, we consider
476 carbonate precipitation unlikely in the batch experiments performed here, and hence, the cause of
477 the $\Delta TA/\Delta Si < 4$ remains unexplained and requires further investigation.

478 Thermodynamic modelling in Griffioen[47] suggests that precipitation of the hydrated
479 phyllosilicate sepiolite ($Mg_4Si_6O_{15}(OH)_2 \cdot 6H_2O$) could reduce $\Delta TA/\Delta Si$ values, thus inducing a
480 lower CO_2 sequestration efficiency of enhanced olivine weathering in seawater. However, no
481 sepiolite was found in the XRD analyses. The extent to which secondary reactions impact the CO_2

sequestration efficiency of olivine dissolution under *in situ* conditions within the seabed remains an important issue to address in further studies on coastal ESW.

Due to the exclusion of Mg^{2+} and Ca^{2+}, the ionic strength of the ASW-CaMg medium was lower than that of the ASW (Table S3). The ionic strength of the ASW was 0.72 mol kg^{-1}, while that of ASW-Ca was 0.015 mol kg^{-1} (or 2%) lower than ASW. Equally, the ionic strength of ASW-CaMg was 0.0975 mol kg^{-1} (or 13%) lower than that of ASW. Ionic strength impacts the activity coefficients of aqueous species and has been found to impact dissolution kinetics, particularly at lower pH [16]. Still, other factors (i.e. pCO_2, pH, saturation state) exhibit a much larger influence on dissolution kinetics[48,49]. Given the relatively high pH in the reactive fluids (pH 7.9-8.2) and the fact that all solutions were highly undersaturated with respect to fosterite, the impact of the lower ionic strength of the ASW-CaMg was likely to be very small.

The rate at which CO_2 is sequestered due to olivine dissolution in seawater can thus be formulated as the following relation:

(7) $$R_{CO_2} = 4\, R_{OLI}\, \gamma_{CO_2} (1-x)$$

Here, 4 denotes the theoretical stoichiometry between olivine dissolution and CO_2 [5,14], R_{OLI} is the olivine dissolution rate, γ_{CO_2} is the reaction efficiency of the CO_2 sequestration in seawater and x is the molar fraction of Fe in the olivine source material.

Olivine application in a coastal geo-engineering framework

In order to place coastal ESW in a broader perspective, a real-world example illustrates its carbon-capturing potential. The Netherlands is a densely-populated, industrialized country, with a GDP of ca. 850 billion USD (2013) and ca. 50 % of its surface area below sea level[50]. To protect the coastal region of the country where ca. 60% of the GDP is produced[51,52], continuous large-scale sand nourishments are needed. Between 2000 and 2010, ca. 12 million m^3 (Mm^3) sand per year have been deployed along the Netherlands' coast, which is expected to increase due to predicted climate change-induced sea level rise[51,52] (https://www.noordzeeloket.nl/en/functions-and-use/surface-

mining-and-quarrying/).

In a thought experiment, the sand used in these coastal nourishments is replaced by finely ground olivine as used in the experiments described here. In a hypothetical one-time application of 12 Mm^3 (≈ 26 Mt) of olivine sand, parameter values for $k_{\Delta TA}$ obtained in our experiments (Table 1) were implemented in the Olsen[53] shrinking core model for olivine carbonation (assuming the measured olivine particle size distribution; see SI 2). This model has been previously implemented in ten Berge et al. [54], describing total mass of olivine weathered and consequential CO_2 captured (SI 8). Our simulations showed a cumulative weathering of 4% of the olivine after the first year, 12% after five years, 35% after 25 years, 57% after 50 years and 84% after 100 years (Fig. 5A). After 200 years, 98% of the initially applied 12 Mm^3 olivine will be dissolved. These values are in accordance with those presented by Hangx and Spiers[14], in which 100 μm (median diameter, D_{50}) olivine grains would take >100 years to dissolve.

Making use of the earlier derived relationship, Eqn. (6) $R_{CO_2}=4\,R_{OLI}\gamma_{CO_2}(1-x)$, with $\gamma_{CO_2}=0.84$ and x = 0.06 as discussed above, the amount of carbon dioxide taken up can be estimated. With annual 12 Mm^3 applications, for periods of 1, 5, 10 and 25 years, the CO_2-capturing rate would increase from ca. 2.5 Mton CO_2 $year^{-1}$ to a peak value of ca. 9 Mton CO_2 $year^{-1}$ after 25 years of coastal olivine application (Fig. 5B). This would be the equivalent of 5% of The Netherlands' yearly 170 Mton CO_2 emissions (2013 value; http://data.worldbank.org/indicator/). Once the application stops, the remaining olivine will dissolve in about 250 years, with decreasing yearly CO_2 uptake rates (Fig. 5B). The long time scale over which ESW is effective has two important implications. Firstly, the process of issuing and validating carbon credits for ESW will need to take into account that CO_2 sequestration is not immediately realized at once, but stretched out over a century-scale time window. Secondly, given the long-lasting effects, any potential ecosystem impacts need to be properly assessed and evaluated upfront in small-scale field trials before large-scale ESW application can start.

Environmental implications

From an ecological perspective, the potential secondary effects of (large-scale) olivine dissolution on the marine ecosystem are a critical issue, and hence it is important (and obligatory in e.g. the European Union) to perform upscaling calculations of dissolution product concentrations and their conceivable effects on the marine ecosystem. The main consequences of forsteritic olivine dissolution are increases in Mg^{2+}, Si, TA, DIC, Fe^{2+} and Ni^{2+}, and their ecosystem effects should be thoroughly assessed. In addition, the geophysical consequences of olivine distribution in coastal ecosystems should be assessed, such as the increase in suspended particulate matter, sediment pore space clogging and smothering effects due to the higher specific density of olivine. While increases in alkalinity and DIC are a desired effect for climate engineering purposes, the increase in Mg^{2+} is not expected to pose a significant threat, because of the high background concentration in seawater. Increases in dissolved Si and dissolved Fe can stimulate primary production, and thus lead to additional CO_2 sequestration, as recently assessed by model analysis[55]. However, the ultimate impacts on coastal foodwebs of fertilizing by olivine dissolution are uncertain and need further investigation.

The impact of increased nickel flux on marine ecosystems is a matter of potential concern, and has only been scarcely touched upon. Although dilution processes in marine coastal environments will likely prevent accumulation to toxic levels of dissolution products, it is important (and obligatory in e.g. the European Union) to perform upscaling calculations of dissolution product concentrations and their conceivable effects on the marine ecosystem.

Nickel leaches from the olivine mineral matrix in its ionic Ni(II) form. Dissolved nickel occurs in trace concentrations in seawater (0.03 – 0.16 μmol kg^{-1}; [27]), as low as 0.002-0.006 μmol kg^{-1} in the central southern North Sea and up to 0.04 μmol kg^{-1} in the Rhine delta area[28]. In comparison, background nickel concentrations in the control treatments ranged between 0.14 μmol

558 kg^{-1} in the FSW in experiment A3 and 0.45 µmol kg^{-1} in experiment A1, while background Ni
559 concentrations in the artificial seawater media in experiment A3 (ASW, ASW-Ca and ASW-CaMg)
560 were an order of magnitude lower, between 0.017 and 0.032 µmol kg^{-1}.

561 The ecotoxicology of nickel in marine organisms and ecosystems is summarized on the
562 website of the UK Marine Special Areas of Conservation (http://www.ukmarinesac.org.uk/) and
563 established for the UK at a chronic concentration of 0.25 µmol L^{-1}. Nickel toxicity has been reported
564 in a number of cases[56–58]: negative effects on spawning in mysiid shrimps at 2.4 µmol L^{-1}, DNA
565 damage with associated physiological and cytotoxic effects in the blue mussel *Mytilus edulis* at 0.3
566 µmol L^{-1}, disrupting ionoregulatory functions in the green crab *Carcinus maenas* between 8.5 and
567 51 µmol L^{-1} in very low-salinity seawater (0.006 PSU) and organ oxidative stress in the killifish
568 *Fundulus heteroclitus*, also mainly in freshwater. However, one of the conclusions of Blewett et al.
569 [57] and Blewett and Wood [58] is that higher, seawater-like salinities (e.g. 30-38) seem to be negatively
570 correlated with Ni-induced effects. In general, higher salinities are inversely correlated with Ni^{2+}
571 seawater concentrations[59]. Although bio-accumulation of nickel in individual organisms occurs,
572 there seems to be little evidence of bio-magnification throughout (marine) foodwebs[27], although
573 Kumblad et al. [60] present results that suggest the contrary. The potential toxicity of nickel, combined
574 with rather large uncertainties about the magnitude and direction of its response effects, make it
575 paramount to further investigate its ecotoxicological effects within the framework of large-scale
576 application of olivine in coastal environments.

577 Containment is not an issue for ESW. Before any field-scale application, there should be
578 proper field trials in quasi-contained conditions, such as mesocosm setups which can be upscaled in
579 e.g. tidal harbor basins. In the case that a meso-scale field trial (~ 100 m^2) would be undertaken,
580 common dredging equipment would be used to apply the olivine into the (coastal) environment. The
581 same equipment and expertise can be used to remove the olivine sand, should any acute unforeseen
582 situation develop.

The CO_2 sequestration induced by ESW is governed by the acid-base thermodynamics of seawater, which are well understood[26,37,38], therefore rendering the containment of CO_2 in the ocean highly predictable. The central premise of ESW is that it increases the ocean's alkalinity, enabling more CO_2 to be dissolved into seawater at any given pCO_2 compared to the situation where no alkalinity is added to the ocean. This CO_2 will be stay dissolved in the ocean (= contained) as long as no other process changes the alkalinity of the ocean. In the ESW, the CO_2 storage reservoir (the ocean) is an open system, as CO_2 can be freely exchanged between atmosphere and ocean across the air-sea interface. As leakage cannot occur in an open system, storage of CO_2 in the ocean is therefore leakage-proof. The proof that CO_2 will be contained for long periods of time is given by observations on the long-term (> 1000 yr) carbon cycle and the impact of natural silicate weathering: the long-term fate of fossil CO_2 is to be absorbed in the ocean[61].

If ESW is applied to coastal systems in a geo-engineering framework, it will be crucial to determine *in situ* olivine dissolution rates, in order to determine the efficiency of the method[42]. Once in the natural sediment, the olivine will be subject to very different biogeochemical and geophysical conditions. Microbial mineralization processes could greatly increase the CO_2 concentration in the sediment's pore waters[62], while benthic macrofauna process vast quantities of sediment for their sustenance and mobility[63,64]. These processes are likely to speed up the dissolution process within marine sediments. Large-scale sediment transport and wave action are expected to cause constant particle abrasion and faster mechanical weathering, in turn facilitating faster chemical weathering. If ever to be applied in a geo-engineering framework, it is of paramount importance to investigate the effects of all these natural processes on the dissolution of olivine in coastal environments.

Acknowledgements

The authors wish to thank Steven Way, Yvonne van der Maas, Jurian Brasser and Peggy Bartsch for their contributions and work in the lab. Diana Vasquez is thanked for the many constructive

discussions on the manuscript. Jens Hartmann is supported by the German Science Foundation DFG (Exc 177 and HA 4471/10-2). Pol Knops was supported by Deltares/Climate KIC. The authors wish to thank the Hercules Foundation (Belgium) for financing the ICP-SF-MS instrument (UABR/11/010). We thank Vanessa of V.GonzalezOrtiz Scientific Illustration & Outreach (http://vgonzalezortiz.com/en/) for the TOC art illustration and other graphic advice and services.

Abbreviations

ESW, Enhanced Silicate Weathering, OA, ocean acidification, OLI olivine treatment, QUA quartz treatment, FSW filtered seawater, ASW artificial seawater, ASW-Ca artificial seawater without calcium, ASW-CaMg artificial seawater without calcium and magnesium, PSU practical salinity units

References

(1) Comittee on Geoengineering Climate; Board on Atmospheric Sciences and Climate; Ocean Studies Board; Division on Earth and Life Studies; National Research Council. *Climate Intervention: Carbon Dioxide Removal and Reliable Sequestration*; Washington DC, USA, 2015.

(2) Gasser, T.; Guivarch, C.; Tachiiri, K.; Jones, C. D.; Ciais, P. Negative emissions physically needed to keep global warming below 2 °C. *Nat. Commun.* **2015**, *6*, 7958.

(3) Sanderson, B. M.; O'Neill, B. C.; Tebaldi, C. What would it take to achieve the Paris temperature targets? *Geophys. Res. Lett.* **2016**, *43* (13), 7133–7142.

(4) UNFCCC. *The 2015 Paris Climate Change Conference: COP21.*; 2016; Vol. 99, pp 97–104.

(5) Schuiling, R. D.; Krijgsman, P. Enhanced Weathering: An Effective and Cheap Tool to Sequester CO2. *Clim. Change* **2006**, *74* (1–3), 349–354.

(6) Hartmann, J.; West, J. A.; Renforth, P.; Köhler, P.; Rocha, C. L. D. La; Wolf-Gladrow, D. A.; Dürr, H. H.; Scheffran, J. Enhanced chemical weathering as a geoengineering strategy to reduce atmospheric carbon dioxide, supply nutirents, and mitigate ocean acidification. *Rev. Geophys.* **2013**, *51* (2012), 113–149.

(7) The Royal Society. *Geoengineering the climate: science, governance and uncertainty*; London, United Kingdom, 2009; Vol. 12.

(8) IPCC. *Climate Change 2014: Synthesis Report. Contribution of Working Groups I, II and III to the Fifth Assessment Report of the Intergovernmental Panel on Climate Change.*; Geneva, Switzerland, 2014.

(9) Taylor, L. L.; Quirk, J.; Thorley, R. M. S.; Kharecha, P. A.; Hansen, J.; Ridgwell, A.; Lomas, M. R.; Banwart, S. A.; Beerling, D. J. Enhanced weathering strategies for stabilizing climate and averting ocean acidification. *Nat. Clim. Chang.* **2015**, *6* (4), 402–406.

(10) Ebelmen, J. J. Sur les produits de la décomposition des espècesminérales de la famille des silicates. *Ann. DES MINES* **1845**, *7*, 3–66.

(11) Renforth, P. The potential of enhanced weathering in the UK. *Int. J. Greenh. Gas Control* **2012**, *10*, 229–243.

(12) Köhler, P.; Hartmann, J.; Wolf-Gladrow, D. A. Geoengineering potential of artificially enhanced silicate weathering of olivine. *Proc. Natl. Acad. Sci. U. S. A.* **2010**, *107* (47), 20228–20233.

(13) Köhler, P.; Abrams, J. F.; Völker, C.; Hauck, J.; Wolf-Gladrow, D. A. Geoengineering Impact of Open Ocean Dissolution of Olivine on Atmospheric CO2, Surface Ocean pH and Marine Biology. *Environ. Res. Lett.* **2013**, *8* (1), 14009.

(14) Hangx, S. J. T.; Spiers, C. J. Coastal spreading of olivine to control atmospheric CO2 concentrations: A critical analysis of viability. *Int. J. Greenh. Gas Control* **2009**, *3* (6), 757–767.

(15) Wogelius, R. A.; Walther, J. V. Olivine dissolution at 25° C: Effects of pH, CO2, and organic acids. *Geochim. Cosmochim. Acta* **1991**, *55* (4), 943–954.

(16) Pokrovsky, O. S.; Schott, J. Kinetics and mechanism of forsterite dissolution at 25°C and pH from 1 to 12. *Geochim. Cosmochim. Acta* **2000**, *64* (19), 3313–3325.

(17) Oelkers, E. H. An experimental study of forsterite dissolution rates as a function of temperature and aqueous Mg and Si concentrations. *Chem. Geol.* **2001**, *175* (3–4), 485–494.

(18) Rosso, J. J.; Rimstidt, D. J. A high resolution study of forsterite dissolution rates. *Geochim. Cosmochim. Acta* **2000**, *64* (5), 797–811.

(19) ASTM International. Standard Practice for the Preparation of Substitute Ocean Water. *D 1141 - 98*. ASTM International, PA, USA: West Conshohocken 1999, pp 98–100.

(20) Nieuwenhuize, J.; Maas, Y. E. .; Middelburg, J. J. Rapid analysis of organic carbon and nitrogen in particulate materials. *Mar. Chem.* **1994**, *45* (3), 217–224.

(21) Milne, A.; Landing, W.; Bizimis, M.; Morton, P. Determination of Mn, Fe, Co, Ni, Cu, Zn, Cd and Pb in seawater using high resolution magnetic sector inductively coupled mass spectrometry (HR-ICP-MS). *Anal. Chim. Acta* **2010**, *665*, 200–207.

(22) Palandri, J. L.; Kharaka, Y. K. *A compilation of rate parameters of water-mineral interaction*

kinetics for application to geochemical modeling; Menlo Park, California, 2004; Vol. 2004–1068.

(23) R Development Core Team. R: A language and environment for statistical computing. R Foundation for Statistical Computing: Vienna, Austria 2008.

(24) Wogelius, R. A.; Walther, J. V. Olivine dissolution kinetics at near-surface conditions. *Chem. Geol.* **1992**, *97* (1–2), 101–112.

(25) Pokrovsky, O. S.; Schott, J. Forsterite surface composition in aqueous solutions: A combined potentiometric, electrokinetic, and spectroscopic approach. *Geochim. Cosmochim. Acta* **2000**, *64* (19), 3299–3312.

(26) Wolf-Gladrow, D. A.; Zeebe, R. E.; Klaas, C.; Körtzinger, A.; Dickson, A. G. Total alkalinity: The explicit conservative expression and its application to biogeochemical processes. *Mar. Chem.* **2007**, *106* (1–2), 287–300.

(27) WHO. *Environmental Health Criteria No. 108 Nickel*; Geneva, 1991.

(28) Burton, J. D.; Althaus, M.; Millward, G. E.; Morris, A. W.; Statham, P. J.; Tappin, A. D.; Turner, A. Processes influencing the fate of trace metals in the North Sea. In *Understanding the North Sea system*; Charnock, H., Dyer, K. R., Huthnance, J. M., Liss, P. S., Simpson, J. H., Tett, P. B., Eds.; Springer Science+Business Media: Dordrecht, NL, 1994; pp 179–190.

(29) Wolff-Boenisch, D.; Wenau, S.; Gislason, S. R.; Oelkers, E. H. Dissolution of basalts and peridotite in seawater, in the presence of ligands, and CO2: Implications for mineral sequestration of carbon dioxide. *Geochim. Cosmochim. Acta* **2011**, *75* (19), 5510–5525.

(30) Hellmann, R.; Wirth, R.; Daval, D.; Barnes, J. P.; Penisson, J. M.; Tisserand, D.; Epicier, T.; Florin, B.; Hervig, R. L. Unifying natural and laboratory chemical weathering with interfacial dissolution-reprecipitation: A study based on the nanometer-scale chemistry of fluid-silicate interfaces. *Chem. Geol.* **2012**, *294–295*, 203–216.

(31) Shannon, R. D. Revised effective ionic radii and systematic studies of interatomic distances in halides and chalcogenides. *Acta Crystallogr. Sect. A* **1976**, *32* (5), 751–767.

(32) Maher, K.; Johnson, N. C.; Jackson, A.; Lammers, L. N.; Torchinsky, A. B.; Weaver, K. L.; Bird, D. K.; Brown, G. E. A spatially resolved surface kinetic model for forsterite dissolution. *Geochim. Cosmochim. Acta* **2016**, *174*, 313–334.

(33) Bearat, H.; McKelvy, M. J.; Chizmeshya, A. V. G.; Gormley, D.; Nunez, R.; Carpenter, R. W.; Squires, K.; Wolf, G. H. Carbon sequestration via asueous olivine mineral carbonation: role of passivating layer formation. *Environ. Sci. Technol.* **2006**, *40* (15), 4802–4808.

(34) Olsson, J.; Bovet, N.; Makovicky, E.; Bechgaard, K.; Balogh, Z.; Stipp, S. L. S. Olivine reactivity with CO2 and H2O on a microscale: Implications for carbon sequestration. *Geochim. Cosmochim. Acta* **2012**, *77*, 86–97.

(35) Garcia, B.; Beaumont, V.; Perfetti, E.; Rouchon, V.; Blanchet, D.; Oger, P.; Dromart, G.; Huc, a.-Y.; Haeseler, F. Experiments and geochemical modelling of CO2 sequestration by olivine: Potential, quantification. *Appl. Geochemistry* **2010**, *25* (9), 1383–1396.

(36) Schott, J.; Brantley, S.; Crerar, D.; Guy, C.; Borcsik, M.; Willaime, C. Dissolution kinetics of strained calcite. *Geochim. Cosmochim. Acta* **1989**, *53* (2), 373–382.

(37) Zeebe, R. E.; Wolf-Gladrow, D. A. *CO2 in Seawater: Equilibrium, Kinetics, Isotopes*; Elsevier Science BV, 2001.

(38) Sarmiento, J. L.; Gruber, N. *Ocean Biogeochemical Dynamics*; Princeton University Press, 2006.

(39) Huettel, M.; Berg, P.; Kostka, J. E. Benthic Exchange and Biogeochemical Cycling in Permeable Sediments. *Ann. Rev. Mar. Sci.* **2014**, *6*, 23–51.

(40) Aller, R. C.; Aller, J. Y. The effect of biogenic irrigation intensity and solute exchange on diagenetic reaction rates in marine sediments. *J. Mar. Res.* **1998**, *56* (4), 905–936.

(41) Rao, A. M. F.; Malkin, S. Y.; Montserrat, F.; Meysman, F. J. R. Alkalinity production in intertidal sands intensified by lugworm bioirrigation. *Estuar. Coast. Shelf Sci.* **2014**, *148*, 36–47.

(42) Meysman, F. J. R.; Montserrat, F. Negative CO2 emissions via enhanced silicate weathering in coastal environments. *Biol. Lett.* **2017**.

(43) Hofmann, A. F.; Middelburg, J. J.; Soetaert, K.; Meysman, F. J. R. pH modelling in aquatic systems with time-variable acid-base dissociation constants applied to the turbid, tidal Scheldt estuary. *Biogeosciences* **2009**, *6* (8), 1539–1561.

(44) Hofmann, A. A. F.; Soetaert, K.; Meysman, F. J. R. AquaEnv - an integrated development toolbox for aquatic chemical model generation. 2012.

(45) Berner, R. A. The role of magnesium in the crystal growth of calcite and aragonite from sea water. *Geochim. Cosmochim. Acta* **1975**, *39* (4), 489–504.

(46) Karoui, H.; Korchef, A.; Tlili, M. M.; Mosrati, H.; Gil, O.; Mosrati, R.; Ben Amor, M. Effects of Mg2+, Ca2+ and SO42- ions on the precipitation kinetics and microstructure of aragonite. *Ann. Chim. DES Mater.* **2008**, *33* (2), 123–134.

(47) Griffioen, J. Enhanced weathering of olivine in seawater: The efficiency as revealed by thermodynamic scenario analysis. *Sci. Total Environ.* **2017**, *575*, 536–544.

(48) Krevor, S. C. M.; Lackner, K. S. Enhancing serpentine dissolution kinetics for mineral carbon dioxide sequestration. *Int. J. Greenh. Gas Control* **2011**, *5* (4), 1073–1080.

(49) Giammar, D. E.; Bruant, R. G.; Peters, C. A. Forsterite dissolution and magnesite precipitation at conditions relevant for deep saline aquifer storage and sequestration of carbon dioxide. *Chem. Geol.* **2005**, *217* (3–4), 257–276.

(50) UNESCO World Water Assessment Programme. *The UN World Water Development Report 3: Water in a Changing World*; Paris, London, 2009.

(51) Mulder, J. P. M. *Zandverliezen in het Nederlandse kustysteem; Advies voor Dynamisch Handhaven in de 21e eeuw (in Dutch)*; The Hague, The Netherlands, 2000.

(52) Mulder, J. P. M.; Hommes, S.; Horstman, E. M. Implementation of coastal erosion

management in the Netherlands. *Ocean Coast. Manag.* **2011**, *54*, 888–897.

(53) Olsen, A. A. Forsterite dissolution kinetics: Applications and implications for chemical weathering, Virginia State University, 2007.

(54) ten Berge, H. F. M.; van der Meer, H. G.; Steenhuizen, J. W.; Goedhart, P. W.; Knops, P.; Verhagen, J. Olivine Weathering in Soil, and Its Effects on Growth and Nutrient Uptake in Ryegrass (Lolium perenne L.): A Pot Experiment. *PLoS One* **2012**, *7* (8), e42098.

(55) Hauck, J.; Köhler, P.; Wolf-Gladrow, D.; Völker, C. Iron fertilisation and century-scale effects of open ocean dissolution of olivine in a simulated CO_2 removal experiment. *Environ. Res. Lett.* **2016**, *11* (2), 24007.

(56) Millward, G. E. .; Kadam, S. .; Jha, A. N. Tissue-specific assimilation, depuration and toxicity of nickel in Mytilus edulis. *Environ. Pollut.* **2012**, *162*, 406–412.

(57) Blewett, T. A.; Glover, C. N.; Fehsenfeld, S.; Lawrence, M. J.; Niyogi, S.; Goss, G. G.; Wood, C. M. Making sense of nickel accumulation and sub-lethal toxic effects in saline waters: Fate and effects of nickel in the green crab, Carcinus maenas. *Aquat. Toxicol.* **2015**, *164*, 23–33.

(58) Blewett, T. A.; Wood, C. M. Salinity-Dependent Nickel Accumulation and Oxidative Stress Responses in the Euryhaline Killifish (Fundulus heteroclitus). *Arch. Environ. Contam. Toxicol.* **2015**, *68* (2), 382–394.

(59) CEFAS. *Monitoring and surveillance of non-radioactive contaminants in the aquatic environment and activities regulating the disposal of wastes at sea, 1994*; Lowestoft, 1997.

(60) Kumblad, L.; Bradshaw, C.; Gilek, M. Bioaccumulation of 51Cr, 63Ni and 14C in Baltic Sea benthos. *Environ. Pollut.* **2005**, *134* (1), 45–56.

(61) Archer, D. Fate of fossil fuel CO2 in geologic time. *Geophys. Res. Lett.* **2005**, *110*, 6.

(62) Burdige, D. J. *Geochemistry of Marine Sediments*; Princeton University Press: New Jersey, 2006.

(63) Meysman, F. J. R.; Middelburg, J. J.; Heip, C. H. R. Bioturbation: a fresh look at Darwin's last idea. *TRENDS Ecol. Evol.* **2006**, *21* (12), 688–695.

(64) Montserrat, F.; Van Colen, C.; Degraer, S.; Ysebaert, T.; Herman, P. M. J. Benthic community-mediated sediment dynamics. *Mar. Ecol. Prog. Ser.* **2008**, *372* (1), 43–59.

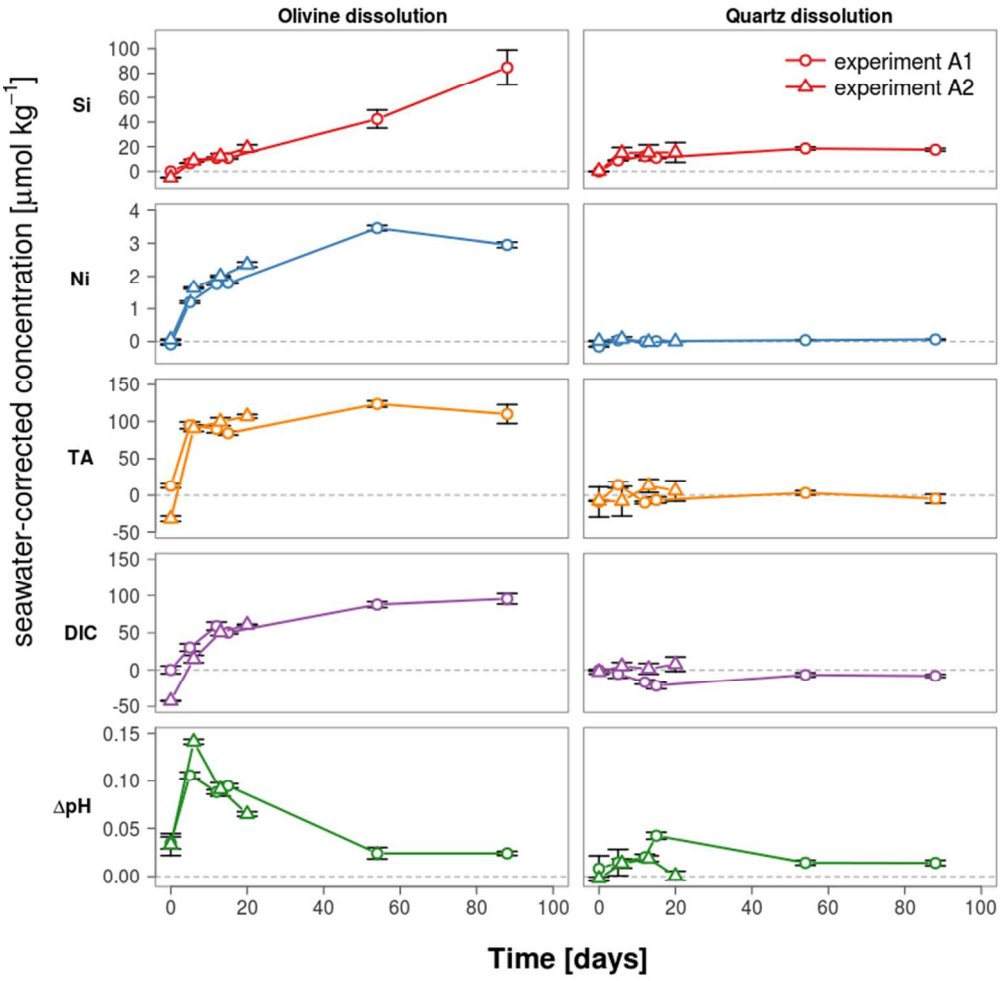

Temporal development of olivine dissolution response variables in experiments A1 and A2. Symbols denote mean seawater-corrected values (see Materials & Methods), with error bars denoting standard error of the mean (SEM). Circles: values from experiment A1; triangles: values from experiment A2. The values for both experiments are plotted with the olivine (OLI) and quartz (QUA) treatments plotted alongside on the same vertical scale for comparison. The reported units are micromole per kg seawater, except for pH, which is in pH units on the Total scale.

Fig. 1

219x218mm (96 x 96 DPI)

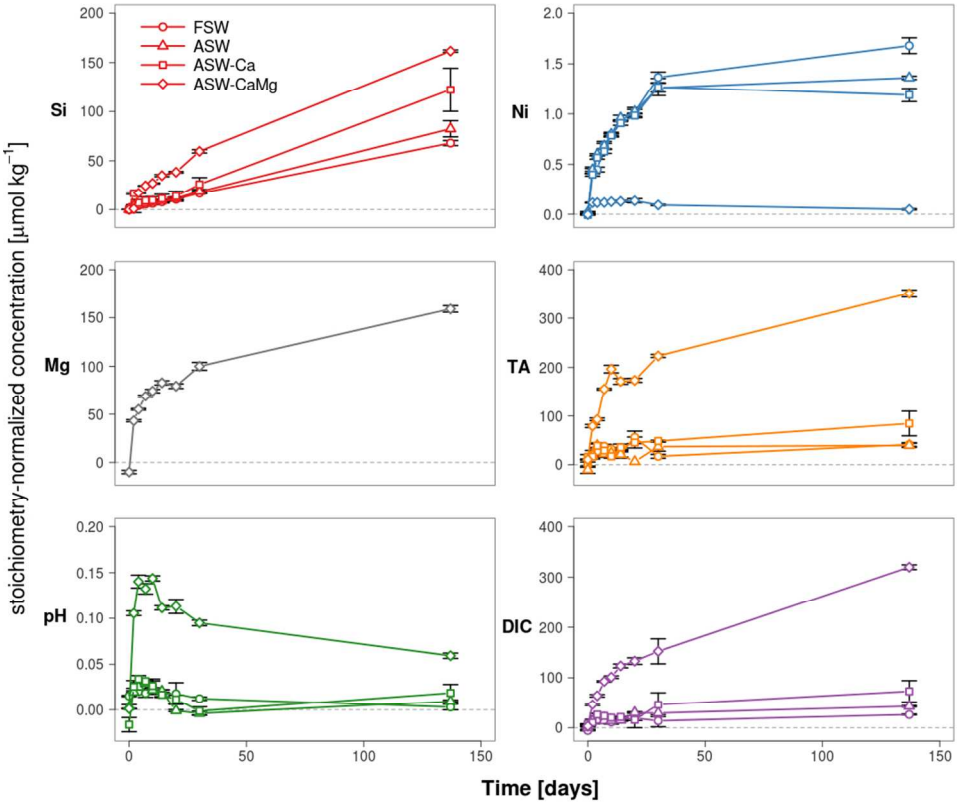

Temporal development of olivine dissolution response variables in experiment A3. Symbols denote mean seawater-corrected values (see Materials & Methods) for the olivine treatment (OLI), with error bars denoting standard error of the mean (SEM). Circles: values from filtered seawater treatment (FSW); triangles: values from artificial seawater treatment (ASW); squares: values from artificial seawater without calcium treatment (ASW-Ca); diamonds: values from artificial seawater without calcium and magnesium treatment (ASW-CaMg). The reported units are micromole per kg seawater (corrected for control values), except for pH, which is in pH units on the Total scale.

Fig. 2

298x243mm (96 x 96 DPI)

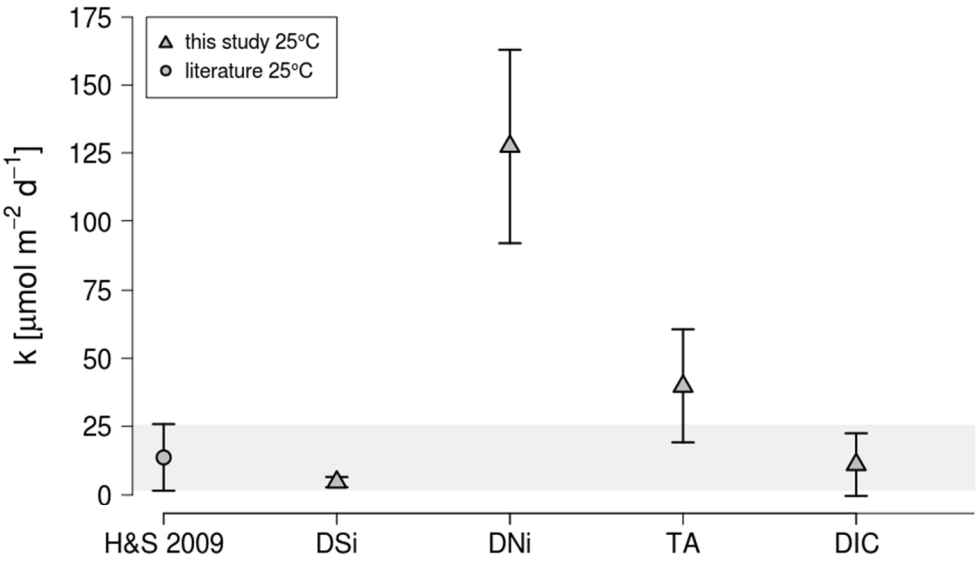

The olivine dissolution rate constant *k*, calculated as the mean (+/- SD) value of the different response variables measured in the three agitation experiments A1, A2 and A3 (Table S4). In order to obtain the most realistic estimates for olivine dissolution in seawater, only values from the FSW and ASW treatments were considered. For comparison, the estimated value by Hangx and Spiers[14] from previous studies (literature, H&S 2009) is given in the same units as the rates obtained in this study. The literature value and range are denoted by the gray circle and the gray area for clarity. The gray triangles represent the values obtained in this study at 17°C, but re-calculated to 25°C, the same standard temperature as the literature estimates.

Fig. 3

238x158mm (96 x 96 DPI)

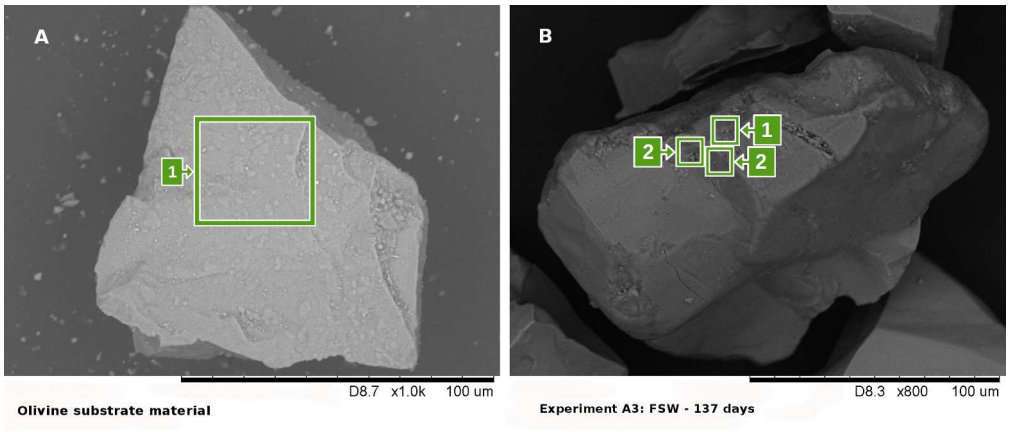

(A) SEM-EDX micrograph of unreacted olivine (substrate material) with very clear angular features and sharp edges. The Mg:Si atomic ratio in area 1 typically lies between 2 and 2.5. (B) SEM-EDX micrograph of an olivine particle after being subjected to continuous movement in FSW during 137 days (experiment A3). On the surface of the same olivine particle, abrupt changes in Mg:Si atomic ratios can be observed within small distances. Areas denoted with 1 are characterized by Mg:Si atomic ratios of 2-2.5, while Mg:Si atomic ratios in areas denoted with 2 showed values of around 1. Such locations, where Mg:Si ratio decreases well below 2, are considered local weathering sites.

Fig. 4

911x388mm (72 x 72 DPI)

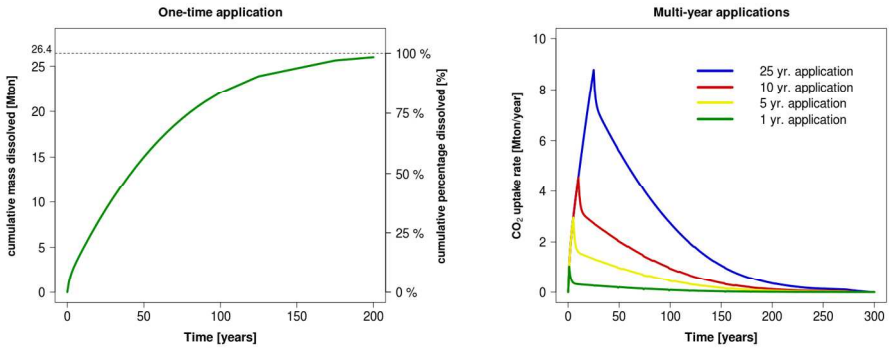

(A) Model results of both absolute and relative cumulative dissolution over time (using dissolution rate constant values as obtained from the experiments in this study), of a one-time hypothetical coastal olivine application of 12 Mm^3, or 26.4 Mton, of olivine sand with the same characteristics as that used here. (B) Model results of the yearly CO_2 uptake rate, as a consequence of hypothetical repeated (multi-year) olivine application as a substitute for yearly coastal sand nourishments during periods of 1, 5, 10 and 25 years.
Fig. 5
508x190mm (96 x 96 DPI)

Table 1

The release rate R^{i}_{max} [µmol kg^{-1} d^{-1}] of each of the measured *i* variables ΔSi, ΔNi, ΔMg, ΔTA and ΔDIC, within each experiment. The number next to each of the R^{i}_{max} values corresponds to the model that best fitted the data (significance of parameters, see methods), where 1=linear model, 2=saturation model, 3=combined model, according to the equations in Table S6.

exp	medium	$R_{\Delta Si}$	$R_{\Delta Ni}$	$R_{\Delta Mg}$	$R_{\Delta TA}$	$R_{\Delta DIC}$
S1	FSW	0.9 [1]	0.2 [3]		39.9 [2]	6.3 [2]
S2	FSW	2.8 [1]	0.4 [2]		52.3 [2]	13.6 [2]
S3	FSW	0.6 [2]	0.1 [3]		11.5 [2]	7.9 [2]
	ASW	0.6 [1]	0.2 [3]		33 [2]	2.10 [2]
	ASW-Ca	0.9 [1]	0.2 [2]		1.6 [2]	1.70 [2]
	ASW-CaMg	3.8 [3]	0.2 [3]	35.4 [3]	32.4 [3]	22.7 [3]

Table 2

The olivine dissolution constant k_i [μmol m^{-2} d^{-1}] based on the R^i_{max} (Table 1) of each of the *i* variables ΔSi, ΔNi, ΔMg, ΔTA and ΔDIC, within each experiment.

exp	solvent	$k_{\Delta Si}$	$k_{\Delta Ni}$	$k_{\Delta Mg}$	$k_{\Delta TA}$	$k_{\Delta DIC}$
S1	FSW	1	31		16	2
S2	FSW	3	56		13	3
S3	FSW	2	60		10	7
	ASW	2	74		28	2
	ASW-Ca	3	65		2	1
	ASW-CaMg	13	65	63	27	19